Assignment Strategies in Homonuclear Three-Dimensional ^{1}H NMR Spectra of Proteins†

G. W. Vuister, R. Boelens, A. Padilla, G. J. Kleywegt, and R. Kaptein*
Department of Chemistry, University of Utrecht, Padualaan 8, 3584 CH Utrecht, The Netherlands
Received July 6, 1989; Revised Manuscript Received October 2, 1989

ABSTRACT: The increase in dimensionality of three-dimensional (3D) NMR greatly enhances the spectral resolution in comparison to 2D NMR. It alleviates the problem of resonance overlap and may extend the range of molecules amenable to structure determination by high-resolution NMR spectroscopy. Here, we present strategies for the assignment of protein resonances from homonuclear nonselective 3D NOE–HOHAHA spectra. A notation for connectivities between protons, corresponding to cross peaks in 3D spectra, is introduced. We show how spin systems can be identified by tracing cross-peak patterns in cross sections perpendicular to the three frequency axes. The observable 3D sequential connectivities in proteins are tabulated, and estimates for the relative intensities of the corresponding cross peaks are given for α-helical and β-sheet conformations. Intensities of the cross peaks in the 3D spectrum of pike III parvalbumin follow the predictions. The sequential-assignment procedure is illustrated for loop regions, extended and α-helical conformations for the residues Ala 54–Leu 63 of parvalbumin. NOEs that were not previously identified in 2D spectra of parvalbumin due to overlap are found.

During the past decade, a wide range of high-resolution NMR[1] techniques have emerged, which have enabled the structure elucidation of numerous biological macromolecules, mostly proteins, with molecular weights of up to approximately 15 000 (Wüthrich, 1986; Kaptein et al., 1988; Vliegenthart et al., 1983). However, with increasing size of these molecules, the spectra have become more complicated. Currently, molecules with a molecular weight of up to 15 000 are amenable to 2D NMR studies. The introduction of a third frequency domain could, in principle, extend this range. Thus, a number of selective and nonselective homonuclear 3D NMR experiments, as well as several heteronuclear 3D NMR experiments, have recently been proposed and performed. In the 3D *J*-resolved experiment, COSY cross peaks are modulated by the *J* couplings, allowing determination of spin multiplets in a third frequency domain (Vuister & Boelens, 1987; Hoffman & Davies, 1988). Homonuclear semiselective COSY–COSY (Griesinger et al., 1987a), NOESY–COSY (Griesinger et al., 1987b), NOESY–HOHAHA (or NOESY–TOCSY) (Oschkinat et al., 1988), and HOHAHA–NOESY (Oschkinat et al., 1989) experiments have been used to record protein spectra in which the chemical shift in the ω_1 domain was restricted to the amide frequency range and that in the ω_2 domain to the $C_\alpha H$ frequency range.

In contrast, in experiments such as the nonselective 3D NOE–HOHAHA (Vuister et al., 1988) and the nonselective 3D NOE–NOE (Boelens et al., 1989), spectra encompassing the whole chemical-shift range along each of the frequency axes were obtained. Their use has been demonstrated on proteins (Vuister et al., 1988) and oligosaccharides (Vuister et al., 1989).

In heteronuclear 3D experiments such as the HMQC–COSY, HMQC–NOESY (Fesik & Zuiderweg, 1988) and the reverse experiment NOESY–HMQC (Zuiderweg & Fesik, 1989; Marion et al., 1989), the chemical-shift dispersion of the ^{15}N or ^{13}C nuclei is used for editing the otherwise complex homonuclear 2D spectra. In these experiments, a series of homonuclear subspectra dependent on the chemical shift of the heteronucleus are obtained. It should be noted that the total number of cross peaks in a heteronuclear 3D spectrum is equal to that in the corresponding homonuclear 2D spectrum, whereas homonuclear 3D spectra yield extra cross peaks that allow the identification of specific interactions in different ways.

We recently reported on a nonselective homonuclear 3D NOE–HOHAHA experiment on pike III parvalbumin, a calcium-binding protein of 109 amino acids (Vuister et al., 1988). The complete assignment of the proton resonances, which represents the main bottleneck in the structure elucidation by high-resolution NMR spectroscopy, can, in principle, be obtained from this experiment. In this paper we will give an outline of an assignment strategy and indicate how a 3D NOE–HOHAHA spectrum can be used to obtain these assignments. We will introduce a notation for 3D connectivities, describing the coherence-transfer pathways, which allows a unique labeling of cross peaks. This notation can easily be adapted to describe any type of 2D or 3D connectivity in a uniform manner. The intensity of a 3D cross peak is intimately correlated with secondary structure elements such as α-helices and β-sheets in which the protons are present. Estimates for 3D cross-peak intensities corresponding to these secondary structure elements will be given. Examples will be given of the sequential assignment of residues in extended conformations, turn regions and α-helical domains, as found in the 3D NOE–HOHAHA spectrum of pike III parvalbumin in H_2O.

Theory

Any 3D NMR experiment can be conceived as a combination of two 2D experiments. The detection period of the

† This work was supported by the The Netherlands Foundation for Chemical Research (SON) with financial aid from The Netherlands Organization for the Advancement of Research (NWO).
* Address correspondence to this author.

[1] Abbreviations: NMR, nuclear magnetic resonance; NOE, nuclear Overhauser enhancement; 2D, two-dimensional; 3D, three-dimensional; NOESY, 2D NOE spectroscopy; COSY, 2D correlation spectroscopy; TPPI, time-proportional phase increment; HOHAHA, homonuclear Hartmann–Hahn spectroscopy; TOCSY, total correlation spectroscopy; HMQC, heteronuclear multiple-quantum correlation; FID, free induction decay.

0006-2960/90/0429-1829$02.50/0

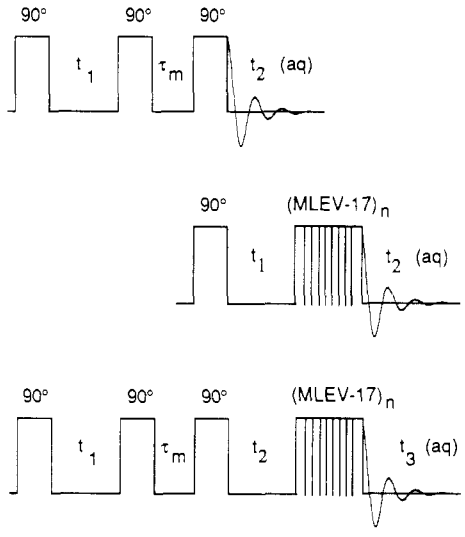

FIGURE 1: Combination of a 2D NOE and a 2D HOHAHA into a 3D NOE–HOHAHA experiment by replacing the detection period of the 2D NOE experiment with the 2D HOHAHA experiment from which the preparation pulse has been omitted.

first 2D experiment is replaced by a second 2D experiment from which the preparation pulse has been omitted (Griesinger et al., 1987a,b). Thus, an experiment is obtained with a preparation sequence, an evolution period t_1, a first mixing process, an evolution period t_2, a second mixing process, and a detection period t_3. This is illustrated in Figure 1 for the combination of a 2D NOE and a 2D HOHAHA into a 3D NOE–HOHAHA experiment. After the time-domain signal in t_3 is recorded as a function of the two independently incremented variables t_1 and t_2 and after 3D Fourier transformation of all three time domains, a spectrum is obtained that is a function of three frequencies. This spectrum can be represented in a cube with axes ω_1, ω_2, and ω_3.

In the 3D frequency space, a body diagonal ($\omega_1 = \omega_2 = \omega_3$) and three cross-diagonal planes (Figure 2a) can be identified. In the cross-diagonal NOE plane ($\omega_2 = \omega_3$) and the HOHAHA plane ($\omega_1 = \omega_2$) information equivalent to that of the corresponding 2D NMR spectra can be found. A unique phenomenon is the cross-diagonal back-transfer plane ($\omega_1 = \omega_3$). This plane contains cross peaks resulting from magnetization transferred in both mixing periods, from a spin **a** to a spin **b** by NOE and back to spin **a** by isotropic mixing. Since magnetization was transferred twice, these cross peaks have intensities that are of the same order of magnitude as those of the "real" 3D cross peaks (i.e., $\omega_1 \neq \omega_2 \neq \omega_3$).

Projecting the 3D NOE–HOHAHA spectrum onto the ω_1, ω_2 plane yields a 2D NOE spectrum, whereas projecting onto the ω_2, ω_3 plane yields a 2D HOHAHA spectrum. Yet another type of 2D spectrum known as (2D) NOESY–TOCSY (Kessler et al., 1988a,b) can be obtained by projecting onto the ω_1, ω_3 plane.

Particularly useful information can be obtained by examining cross sections perpendicular to one of the frequency axes ω_1, ω_2, or ω_3. Such cross sections will be denoted ω_1, ω_2, and ω_3 cross sections, respectively. Each of these three types of cross section will intersect with the three cross-diagonal planes, yielding three lines called the NOE, HOHAHA, and back-transfer lines. This is illustrated in Figure 2b for a ω_3 cross section. The three lines also intersect at the diagonal point ($\omega_1 = \omega_2 = \omega_3$) of the cross section. These lines are useful mental aids in the process of analyzing the data. This is illustrated in Figure 3 for a ω_1 and a ω_3 cross section. In a ω_1 cross section, those cross peaks will be visible that originate

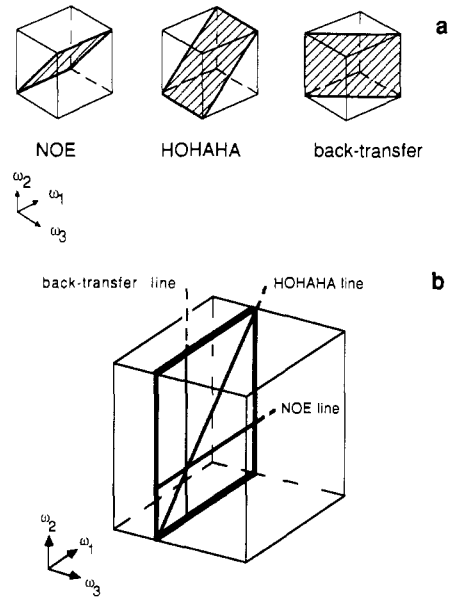

FIGURE 2: 3D spectrum represented in a cube with axes ω_1, ω_2, and ω_3. (a) Cross-diagonal NOE plane ($\omega_2 = \omega_3$), HOHAHA plane ($\omega_1 = \omega_2$), and back-transfer plane ($\omega_1 = \omega_3$). (b) Cross sections perpendicular to ω_3 axis. The cross sections intersect with the three cross-diagonal planes, resulting in three lines indicated as NOE, HOHAHA, and back-transfer line. The three lines also intersect at the diagonal point ($\omega_1 = \omega_2 = \omega_3$) of the cross section. These lines are useful mental aids in the process of analyzing the data.

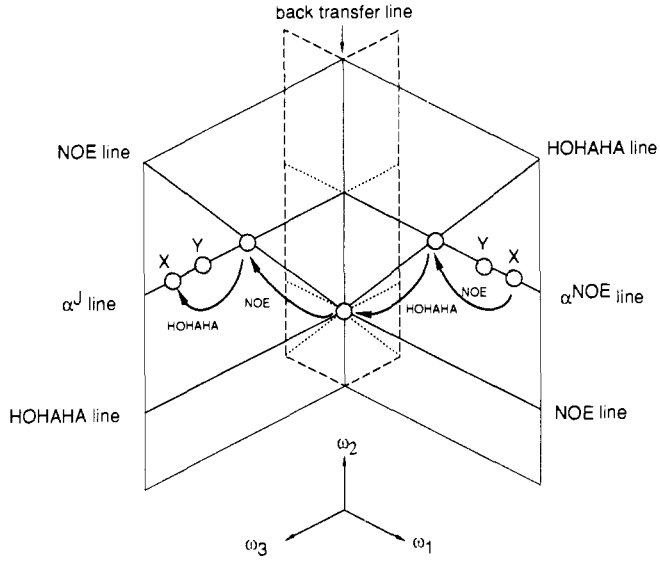

FIGURE 3: Cross sections perpendicular to the ω_1 and ω_3 axes in the 3D frequency space. The connections of cross peaks are indicated by arrows and explained in the text.

from magnetization which was frequency labeled during the first evolution period with the frequency of the particular cross section. Magnetization was then transferred during the NOE mixing period and again frequency labeled during t_2. This is indicated by the arrow from the diagonal point, say at an NH frequency, along the NOE line, for instance to a C_α proton. Subsequent transfer during the HOHAHA mixing period and detection during the t_3 acquisition are indicated by the arrow along the line labeled α^J, parallel to the HOHAHA line of the ω_1 cross section. This line connects protons of the same amino acid residue to the C_α proton.

An ω_3 cross section contains cross peaks that originate from magnetization that was detected at the frequency of the cross section during the t_3 acquisition period. The "reading" of such cross sections will therefore be opposite to that of ω_1 cross

sections. The NOE transfer is indicated by the arrow along the α^{NOE} line parallel to the NOE line in the cross section, followed by the HOHAHA transfer indicated by the arrow to the diagonal point along the HOHAHA line. No similar, simple visualization of transfer pathways can be made for ω_2 cross sections, since in this case the frequency of the cross sections represents the frequency of the intermediate spins of the transfer pathways. However, inspection of ω_2 cross sections can still be usefull as will be demonstrated.

Intensities of 3D Cross Peaks. The intensity of a 3D cross peak depends on the transfer efficiencies of the NOE mixing period τ_m and the HOHAHA mixing period τ_H. The 3D cross-peak intensity is related to the total transfer efficiency $E_{3D}(abc)$, which can be written as a product of the transfer efficiencies of both mixing processes:

$$E_{3D}(abc) = E_{NOE}(ab)E_{HOHAHA}(bc) \quad (1)$$

During the NOE mixing period τ_m the transfer of magnetization between spin **a** and **b** $E_{NOE}(ab)$ for a simple two-spin system can be approximated in the slow-motion limit, assuming a rigid, isotropically tumbling molecule (Noggle & Schirmer, 1971) by

$$E_{NOE}(ab) = E_{NOE}(\text{ref})(r_{ab}/r_{ref})^{-6} \quad (2)$$

where $E_{NOE}(\text{ref})$ represents the NOE transfer corresponding to a reference distance r_{ref} and r_{ab} represents the distance between spins **a** and **b**.

During the isotropic mixing period, τ_H, in-phase magnetization transfer takes place. For a two-spin system this results in oscillatory transfer of coherence between spins **b** and **c** (Braunschweiler & Ernst, 1983). The efficiency of this transfer $E_{HOHAHA}(bc)$ can be approximated by

$$E_{HOHAHA}(bc) \sim \sin^2(\pi J_{bc}\tau_H)R(\tau_H) \quad (3)$$

in which $R(\tau_H)$ describes the relaxation during τ_H. Assuming this relaxation term to be identical for all spins and scaling to a reference value, expression 3 becomes

$$E_{HOHAHA}(bc) = E_{HOHAHA}(\text{ref})[\sin^2(\pi J_{bc}\tau_H)/\sin^2(\pi J_{ref}\tau_H)] \quad (4)$$

The 3D cross-peak transfer efficiency $E_{3D}(abc)$ can then be expressed as

$$E_{3D}(abc) = E_{3D}(\text{ref})(r_{ab}/r_{ref})^{-6}[\sin^2(\pi J_{bc}\tau_H)/\sin^2(\pi J_{ref}\tau_H)] \quad (5)$$

with

$$E_{3D}(\text{ref}) = E_{NOE}(\text{ref})E_{HOHAHA}(\text{ref}) \quad (6)$$

Although expression 4 was derived from a two-spin approximation, we believe it can also be used for estimating the efficiency of the transfer between two spins in a multispin system provided that $2J\tau_H \leq 1$. The largest coupling constants that determine cross-peak intensities relevant for secondary structure determination are ca. 10 Hz, which corresponds to a maximum τ_H of 50 ms. In fact, eq 5 shows that the 3D cross-peak transfer efficiencies are more strongly dependent on the distance r_{ab} than on the coupling constant J_{bc}, so that deviations from the $\sin^2$ behavior become relatively less important.

C Notation for Connectivities in 3D NMR Spectra. It is desirable to have a notation describing connectivities between protons involved in the coherence transfer in 3D NMR experiments. We note that there is a one-to-one mapping of these connectivities onto the 3D cross peaks. For this purpose we propose the notation

$C[x,y]_{abc}(i,j,k)$ with $x, y \in \{\text{NOE, J, ...}\}$ and $a, b, c \in \{\text{N, } \alpha, \beta, \text{...}\}$ and i, j, k are residue numbers

or shorthand

$$C_{abc}(i,j,k)$$

The x,y indication between the square brackets represents the first and second mixing process in the 3D NMR experiment, respectively, e.g., NOE or J coupling (for HOHAHA, COSY, etc.). The subscripts a, b, and c identify the spins in the residues i, j, and k, respectively, that are involved in the pathway. In the case of proteins, a, b, and c may be the amide, C_α, and C_β protons and so on, indicated by N, α, β, etc. However, the notation can also be used in the case of other molecules such as oligosaccharides or DNA fragments by using identifiers that are appropriate to the types of spin that occur in such molecules.

The C notation represents an allowed coherence-transfer pathway of spin **a** of residue i to spin **b** of residue j by the mixing process x, followed by the transfer to spin **c** of residue k by the mixing process y. In this context, it will be referred to as a C pathway. Naturally, the indices x and y can be omitted if the nature of the experiment is known from the context.

This notation can be adapted to 2D NMR spectra by omitting the index y between the square brackets and the last spin and residue identifiers. For C[NOE] pathways it then bears direct resemblance to the $d_{ab}(i,j)$ notation introduced by Wüthrich (1984) for short interproton distances in proteins. However, each distance definition $d_{ab}(i,j)$ introduces two C pathways, i.e., one from a spin **a** to a spin **b** and one from a spin **b** to a spin **a**. In terms of 2D C pathways they could then be noted as $C[\text{NOE}]_{ab}(i,j)$ and $C[\text{NOE}]_{ba}(j,i)$. Obviously, they represent the same connectivity, and the identification by two pathways is in fact redundant.

In a similar way, it can easily be seen that a nonselective 3D NOE–HOHAHA experiment will in principle contain the same information as a nonselective 3D HOHAHA–NOE experiment. Each $C[\text{NOE},J]_{abc}(i,j,k)$ pathway in an NOE–HOHAHA experiment will give rise to a $C[J,\text{NOE}]_{cba}(k,j,i)$ pathway in a HOHAHA–NOE experiment since both pathways represent the same connectivity. Thus, ω_1 cross-section information of the NOE–HOHAHA experiment can be found in the corresponding ω_3 cross section of the HOHAHA–NOE experiment and vice versa. To facilitate the use of the C notation as a *connectivity* notation that is independent of the type of experiment, we propose as a default to substitute NOE and J for the indices x and y, respectively.

Identification of Spin Systems. The identification of spin systems represents one of the major tasks in the assignment of high-resolution NMR spectra. In this section we show how the information from isotropic mixing in a 3D NOE–HOHAHA spectrum can be used to identify spin systems. Obviously, the HOHAHA plane of the 3D spectrum contains this kind of information, but the problem of peak overlap will be as serious as in a 2D spectrum. If one wishes to take full advantage of the 2D resolution, the patterns in the 3D frequency space need to be analyzed.

We shall focus on homonuclear nonselective 3D NOE–HOHAHA spectra of proteins, recorded in H_2O. However, the arguments for its symmetry-related counterpart, the 3D HOHAHA–NOE spectrum, are very similar. We shall begin with a simple case and will subsequently consider overlapping resonances.

The analysis amounts to a search for connectivities between amide, C_α, C_β, and other protons within a spin system. An

ω_3 cross section at an NH frequency could be a starting point (see Figure 3). The use of NH cross sections has the advantage of the generally larger chemical shift dispersion of the amide protons compared to the chemical shift dispersion of the C_α protons. Furthermore, all the cross peaks in a ω_3 cross section, except those on the NOE line, result from at least one transfer step by isotropic mixing involving the amide proton. They therefore establish a correlation between the NH resonance and another resonance within one spin system.

A cross peak in the α-region of the HOHAHA line (diagonal in the ω_3 cross section, see Figure 3) establishes a candidate for the C_α proton. On the α^{NOE} line at this position (parallel to the NOE line of the cross section), NOEs to this potential C_α proton are found. Thus, the $C_{N\alpha N}(i,i,i)$(back-transfer) from its own NH proton may be present, as well as other cross peaks $C_{q\alpha N}(j,i,i)$, where q represents any other spin. One would expect to find at least a number of intraresidue NOEs. The sequential connectivity $C_{N\alpha N}(i+1,i,i)$ is expected in the NH region of this α^{NOE} line. This and other sequential connectivities will later be used in the sequential-assignment process for linking neighboring spin systems. The complete scheme of possibilities will be discussed shortly. A similar reasoning can be applied to the cross peaks in the aliphatic region of the cross section, possibly allowing identification of the C_β proton(s) or any other proton of the spin system.

The ω_1 cross section at the NH frequency gives further information (see also Figure 3). The diagonal in this cross section now represents the NOE line. On this line, the NOE from the NH to the $C_\alpha H$ can be found. The α^J line, parallel to the HOHAHA line, now indicates subsequent transfer during the isotropic mixing period, and thus other resonances in the spin system can be identified.

At this stage, connectivities between the NH, the $C_\alpha H$, and possibly the $C_\beta H$ resonances of the spin system may have been established. The cross sections at the $C_\alpha H$ and $C_\beta H$ resonance frequencies can now be explored in a similar fashion to trace other resonances within the spin system. This procedure can recursively be repeated until it does not yield any new resonances. In addition, new resonances can be correlated with previously identified ones. For instance, in a cross section at the $C_\alpha H$ frequency correlation with the NH frequency is expected to be present. These cross-checks provide a test for internal consistency, as will become clear when the case of overlapping resonances is considered.

If none of the resonances in the spin system overlaps with those of any other spin system, the information that can be extracted is highly redundant. A spin system for which three spins overlap with a second spin system will be indistinguishable for these resonances. However, it is interesting to consider the cases of one- and two-spin overlap. Suppose that there are two or more spin systems with amide protons with identical chemical shifts, but different $C_\alpha H$ resonance frequencies. In this case the ω_3 NH cross section will yield α^{NOE} lines at two or more positions. Naturally, the ω_1 NH cross sections also will yield two or more α^J lines. Clearly, assignment according to the scheme presented above enables one to resolve the ambiguity due to the overlap.

The case of two-spin overlap (e.g., two spin systems that have both identical NH and $C_\alpha H$ resonance frequencies) is more complicated. It will be impossible to assign NOE or HOHAHA cross peaks uniquely to either one of the NH resonances from the α^{NOE} or α^J line alone. The 3D cross peaks on these horizontal lines need not originate from one spin system. Careful examination of all the cross sections will then yield the appropriate correlations. Suppose there could be two spin systems, NH, $C_\alpha H$, $C_x H$ and NH, $C_\alpha H$, $C_y H$, for which both NH and $C_\alpha H$ overlap. The ω_1 and ω_3 cross sections at the NH and $C_\alpha H$ frequencies would suggest NH, $C_\alpha H$, $C_x H$, $C_y H$ correlation (see Figure 3). However, the absence of $C_x H$–$C_y H$ correlations in $C_x H$ or $C_y H$ cross sections would indicate the possibility of a two-spin overlap situation.

Table I: Connectivities in Secondary Structure Elements of Proteins

based on	C[NOE,J]	α-helix[d]	β sheet[d]	
			intrastrand	interstrand
$d_{\alpha N}$	$C_{N\alpha N}(i+1,i,i)$	w	s	
	$C_{N\alpha\alpha}(i+1,i,i)$[a]			
	$C_{N\alpha\beta}(i+1,i,i)$[c]	w–m	m–s	
	$C_{\alpha NN}(i-1,i,i)$[a]			
	$C_{\alpha NN}(i-1,i,i)$[a]			
	$C_{\alpha N\alpha}(i-1,i,i)$	w	s	
	$C_{\alpha N\beta}(i-1,i,i)$[c]	w	m–s	
$d_{\beta N}$	$C_{N\beta N}(i+1,i,i)$[b,c]	v	w–m	
	$C_{N\beta\alpha}(i+1,i,i)$[b,c]	v	w–m	
	$C_{N\beta\beta}(i+1,i,i)$[a,b]			
	$C_{\beta NN}(i-1,i,i)$[a,b]			
	$C_{\beta N\alpha}(i-1,i,i)$[b]	w–m	w–m	
	$C_{\beta N\beta}(i-1,i,i)$[b,c]	w–m	w–m	
d_{NN}	$C_{NNN}(i+1,i,i)$[a]			
	$C_{NN\alpha}(i+1,i,i)$	m	w	
	$C_{NN\beta}(i+1,i,i)$[c]	w–m	w	
	$C_{NNN}(i-1,i,i)$[a]			
	$C_{NN\alpha}(i-1,i,i)$	m	w	
	$C_{NN\beta}(i-1,i,i)$[c]	w–m	w	
$d_{\alpha N}(i,i+3)$	$C_{N\alpha N}(i+3,i,i)$	w		
	$C_{N\alpha\alpha}(i+3,i,i)$[a]			
	$C_{N\alpha\beta}(i+3,i,i)$[c]	w–m		
	$C_{\alpha NN}(i-3,i,i)$[a]			
	$C_{\alpha N\alpha}(i-3,i,i)$	w		
	$C_{\alpha N\beta}(i-3,i,i)$[c]	w		
$d_{\alpha\alpha}(i,j)$	$C_{\alpha\alpha N}(j,i,i)$			s
	$C_{\alpha\alpha\alpha}(j,i,i)$[a]			
	$C_{\alpha\alpha\beta}(j,i,i)$			m–s
$d_{\alpha N}(i,j)$	$C_{N\alpha N}(j,i,i)$			m
	$C_{N\alpha\alpha}(j,i,i)$[a]			
	$C_{N\alpha\beta}(j,i,i)$[c]			w–m
	$C_{\alpha NN}(j,i,i)$[a]			
	$C_{\alpha N\alpha}(j,i,i)$			m
	$C_{\alpha N\beta}(j,i,i)$[c]			w–m

[a] Pathways that give rise to cross-diagonal peaks in the NOE plane. [b] Intensities of cross peaks corresponding to these pathways are strongly dependent on the intervening torsion angle χ. [c] Intensities of cross peaks corresponding to these pathways are dependent on the $^3J_{\alpha\beta}$ coupling constant in residue i. [d] Relative 3D cross-peak intensities corresponding to the listed connectivities in proteins for α-helices and β-sheets are calculated on basis of eq 5, with values for the $d_{\alpha N}$, $d_{\beta N}$, d_{NN}, $d_{\alpha\alpha}(i,j)$, and $d_{\alpha N}(i,j)$ distances taken from Wüthrich (1986) and the $^3J_{\alpha N}$ and $^3J_{\alpha\beta}$ coupling constants from Wüthrich (1986) and Roberts and Jardetzky (1970). Intensities are scaled to a $C_{xyz}(j,i,i)$ peak with r_{xy} = 0.22 nm, and J_{yz} = 10.0 Hz, and τ_H = 50 ms. w < 0.05 ≤ m < 0.5 < s; v = variable.

Effects of Secondary Structure. An essential step in the sequential assignment procedure for protein spectra involves the connection of spin systems using NOEs that correspond to the short distances $d_{\alpha N}$, $d_{\beta N}$, and d_{NN} (Wüthrich, 1986). Naturally, these connectivities can be identified from the 2D-like cross peaks in the cross-diagonal NOE plane, but even more unambiguous information can be obtained by analysis of the "real" 3D cross peaks. The intensities of these cross peaks depend strongly on the secondary structure. On the basis of knowledge about the short-range and medium-range distances $d_{\alpha N}(i,j)$, $d_{\beta N}(i,j)$, and $d_{NN}(i,j)$ for α-helices and antiparallel β-sheets and the long-range distances $d_{\alpha\alpha}(i,j)$ and $d_{\alpha N}(i,j)$ for anti-parallel β-sheets in proteins (Wüthrich, 1984), we can predict the relative intensities of 3D cross peaks that represent sequential connectivities. The results of such an analysis for the amide, C_α, and C_β protons of three neighboring residues are presented in Table I. Some of these pathways

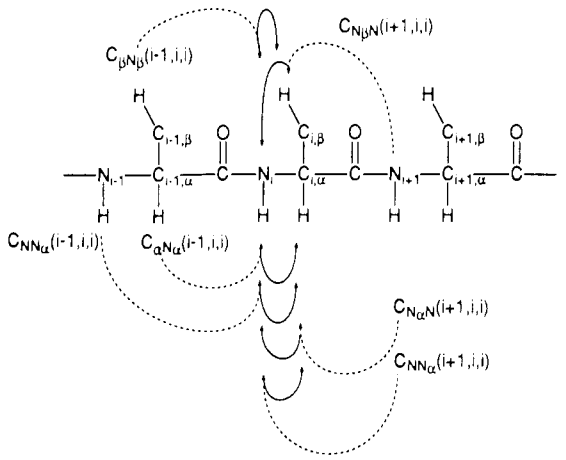

FIGURE 4: Six 3D sequential connectivities mapped onto a part of the primary structure of a protein. Broken arrows represent the magnetization transfer by NOE, whereas solid arrows represent the subsequent transfer by isotropic mixing.

(indicated by the superscript *a* in Table I) represent 2D NOE connectivities and the corresponding cross peaks are located in the cross-diagonal NOE plane. The remaining ones correspond to real 3D cross peaks. Six of these connectivities have been mapped onto the primary structure of a protein in Figure 4 as an illustration. For special cases such as glycine and proline, similar tables can be constructed. For example, in the case of proline, the role of the amide proton is often adopted by one of the C_δ protons (Wüthrich, 1986).

As discussed before, the intensities of the 3D cross peaks depend on the proton–proton distances and the magnitude of the *J* coupling constants. They can be estimated by using eq 5. $^3J_{\alpha N}$ coupling constants for extended conformations are in the range 8–10 Hz, and the $d_{\alpha N}(i,i+1)$ distances are short (0.22 nm). Strong 3D cross peaks are therefore expected for $C_{N\alpha N}$ and $C_{\alpha N\alpha}$ connectivities. In contrast, α-helical domains are characterized by short $d_{NN}(i,i\pm1)$ and sometimes short $d_{\beta N}$ and longer $d_{\alpha N}$ distances and associated with a small $^3J_{\alpha N}$ coupling constant of about 4 Hz. Thus, 3D cross peaks resulting from pathways of protons in α-helical domains are expected to be generally weaker than those resulting from pathways of protons in extended conformations. Some estimates are given in Table I for α-helical and β-sheet conformations. Values for the cross peaks that are based on $d_{\beta N}(i,j)$ distances are strongly dependent on the intervening torsion angle χ.

Sequential Assignment. We shall now discuss how these connectivities can be traced in 3D NMR spectra of a protein. A search for sequential connectivities can be carried out most conventiently in cross sections of the 3D spectrum. These cross sections can be labeled according to their direction (perpendicular to ω_1, ω_2, or ω_3) and chemical-shift value or, equivalently, type of proton such as NH, $C_\alpha H$, or $C_\beta H$. For example, consider the sequential connectivities that can be detected in an ω_3 cross section of a nonselective 3D NOE–HOHAHA experiment at the NH frequency of residue *i*. The $C_{N\alpha N}(i+1,i,i)$ and $C_{N\beta N}(i+1,i,i)$ connectivities of Table I represent real 3D cross peaks. They will be located in the NH region on the α^{NOE} and β^{NOE} lines, respectively. These connectivities are indicated schematically in Figure 5a. In addition, there are the cross-diagonal $C_{\alpha NN}(i-1,i,i)$, $C_{\beta NN}(i-1,i,i)$, $C_{NNN}(i+1,i,i)$, and $C_{NNN}(i-1,i,i)$ connectivities located on the NOE line of the cross section. These are not indicated in Figure 5a.

In Figure 5 the real 3D sequential connectivities in a nonselective 3D NOE–HOHAHA experiment are shown for ω_3 cross sections at the N_iH frequency, the $C_{i,\alpha}H$ frequency, and the $C_{i,\beta}H$ frequency, respectively. A common characteristic of the panels of Figure 5 is that all arrowheads end in the shaded box (ω_3 cross sections). Different selections through the 3D frequency space are provided by ω_1 or ω_2 cross sections. The sequential connectivities of Table I for ω_2 cross sections at the N_iH, $C_{i,\alpha}H$, and $C_{i,\beta}H$ frequencies can be found in Figure 6. Note that the kinks of the arrows are now in the shaded areas, as would be expected for ω_2 cross sections, since these are the cross sections at the frequency of the intermediate spin.

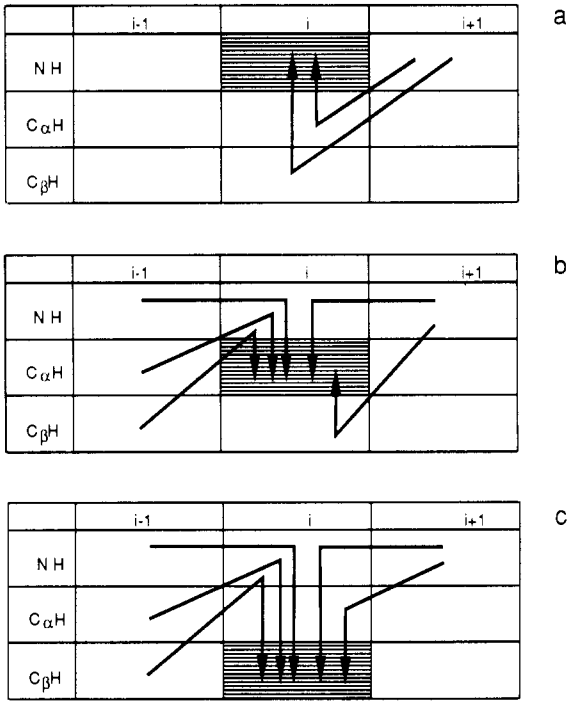

FIGURE 5: 3D sequential connectivities from Table I in a nonselective 3D NOE–HOHAHA experiment for ω_3 cross sections at the N_iH frequency (a), the $C_{i,\alpha}H$ frequency (b), and the $C_{i,\beta}H$ frequency (c).

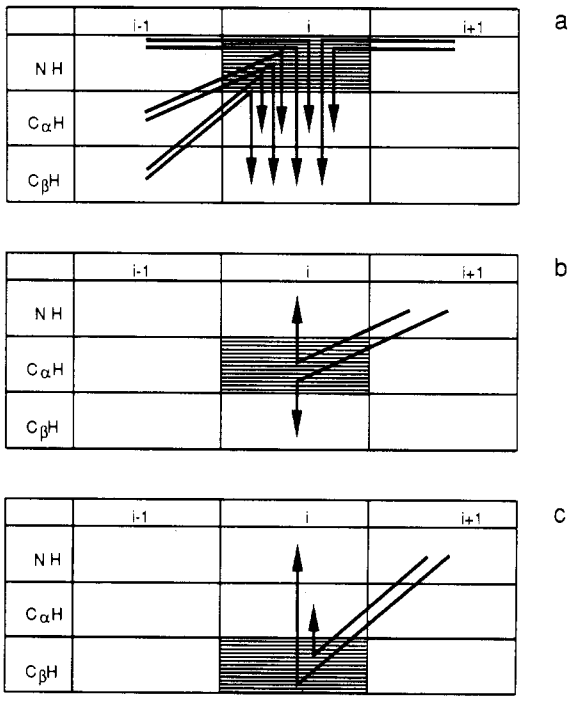

FIGURE 6: 3D sequential connectivities from Table I in a nonselective 3D NOE–HOHAHA experiment for ω_2 cross sections at the N_iH frequency (a), the $C_{i,\alpha}H$ frequency (b), and the $C_{i,\beta}H$ frequency (c).

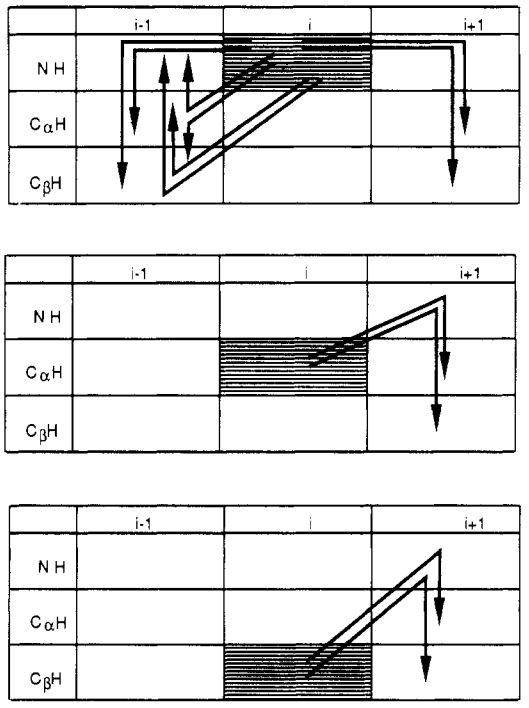

FIGURE 7: 3D sequential connectivities from Table I, after $i-1$ or $i+1$ is substituted for the index i, in a nonselective 3D NOE–HOHAHA experiment for ω_1 cross sections at the N_iH frequency (a), the $C_{i,\alpha}H$ frequency (b), and the $C_{i,\beta}H$ frequency (c).

The ω_1 cross sections (Figure 7) contain connectivities represented by arrows that now originate in the shaded areas. For example, the sequential connectivities that can be identified in an ω_1 cross section at an N_iH frequency comprise the subsets $C_{Nqr}(i,i+1,i+1)$ and $C_{Nqr}(i,i-1,i-1)$, with q and r representing either α, β, or N. In Figure 7, the connectivities of Table I are ordered, after $i-1$ or $i+1$ is substituted for the index i, for ω_1 cross sections at the N_iH frequency, the $C_{i,\alpha}H$ frequency, and the $C_{i,\beta}H$ frequency, respectively.

It should be noted that in each of the Figures 5–7 the 12 arrows represent the *same* connectivities. The rationale for use of the different schemes for the various cross sections is that they provide a convenient way of categorizing the possible connectivities (and, therefore, cross peaks) in a given cross section. In the search for cross peaks in the actual sequential-assignment process these schematic representations proved to be useful visual aids.

The procedure used in the sequential assignment is explained in Figure 8 for ω_3 NH cross sections of two adjacent amino acid residues in the polypeptide chain. The first panel contains the ω_3 cross section at the NH frequency of residue i. The $C_\alpha H$ resonance is found on the HOHAHA line. As can be seen from Figure 5a, the connectivity present in this cross section involving the C_α proton is $C_{N\alpha N}(i+1,i,i)$. The corresponding cross peak can be found in the NH region of the α^{NOE} line. A vertical arrow at the ω_1 axis makes the connection to the ω_3 cross section of the $N_{i+1}H$ resonance. Naturally, the other cross sections (ω_1 or ω_2) can be used in a similar fashion as will be demonstrated for the sequential assignment of residues 54–63 of parvalbumin.

Materials and Methods

The NMR sample was prepared as described previously (Padilla et al., 1988). The protein concentration was 8.7 mM in a 90/10 (v/v) H_2O/D_2O mixture at pH 4.1 at 315 K.

The 3D NOE–HOHAHA spectrum was recorded at 500 MHz on a Bruker AM500 spectrometer, equipped with an

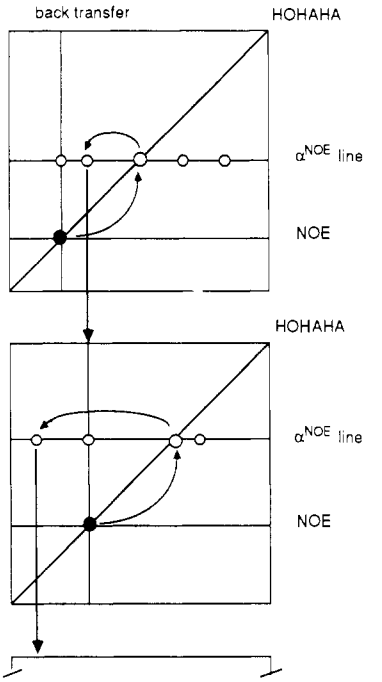

FIGURE 8: Illustration of the sequential-assignment procedure for ω_3 NH cross sections of two adjacent amino acid residues in the polypeptide chain. Arrows now indicate the "line of reasoning" used in the sequential assignment. Refer to the text for further details.

Aspect 3000 computer. For each FID eight scans were taken with the phase cycle of Vuister et al. (1988), preceded by two dummy scans. The FIDs of 512 words were recorded with the carrier in the middle of the spectrum. Independent time-proportional phase increment (Marion & Wüthrich, 1983) was used on the 90° pulses prior to t_1 and t_2 to separate positive and negative frequencies in these domains.

During the relaxation delay of 0.6 s and the NOE mixing time, the H_2O line was suppressed by irradiation. This was repeated for 256 t_2 values and 208 t_1 values, resulting in a total measuring time of 170.5 h. The spectral width in all domains was 6250 Hz. The mixing time τ_m to allow for NOE magnetization transfer was 150 ms. An $(MLEV\text{-}17)_n$ sequence of 47.2 ms, including two trim pulses of 2 ms at the beginning and end of the MLEV mixing time, was used for homonuclear Hartmann–Hahn transfer (Bax & Davis, 1985; Davis & Bax, 1985).

The experimental dataset of 208 × 256 × 512 real points was processed on a microVAX II using software written in FORTRAN 77. To avoid the need for transposition of this large dataset from one domain to another, a data structure based on submatrices was used. This enables fast access to the data in all three dimensions. The data were zero-filled once in the t_2 and t_1 time domains prior to the Fourier transformations. Cosine-bell windows were used in all three time domains. Windowing, Fourier transformation, and phasing of all three time domains took a total processing time of 12.5 h. The data were base-line corrected in all frequency domains independently by an automatic base-line correction algorithm (Boelens et al. 1985) using a third-order polynomial fit, which took another 7.5 h of processing time.

A 3D extension to the ridge-suppression method of Klevitt (1985) and the noise-suppression method of Zolnai et al. (1986) was used to obtain ω_1 and ω_2 "ridge" (average) and "noise" (rms) planes. By use of empty regions of the spectrum along the ω_1 and ω_2 axes, respectively, average and rms values of the base line were calculated, which were used for correction of the spectrum. The resulting real spectral dataset contained

256 × 256 × 256 points. A small fraction of the data points were selected for display on an Evans & Sutherland PS300 picture system. This allowed us to obtain a general overview of the 3D spectrum. For interpretation, however, contour plots of cross sections perpendicular to all three axes were used.

Practical Considerations

As can be expected with any experimental technique, theoretical considerations are sometimes obscured by experimental limitations. We will discuss some of these problems and indicate how they might be overcome.

Long-term instabilities well-known from 2D NMR spectroscopy are expected to be even more important in 3D NMR experiments due to the prolonged experimental time. Temperature fluctuations, deteriorating field homogeneity, and H_2O suppression will lead to t_1 and t_2 artifacts in the 3D NMR spectrum. The t_1,t_2 noise (equivalent to t_1 noise in 2D NMR spectra) will be spread inhomogeneously over the 3D spectrum and may generally be expected to be different in ω_1 and ω_2 due to the different sampling time scales in t_1 and t_2 in the experiment. However, we generally observe a uniform distribution of noise in ω_3 cross sections, dependent on the signal height and line width of the resonances at the frequency of the cross section. This indicates that random instabilities such as phase and amplitude variation of the pulses are mainly responsible for the t_1,t_2 noise.

The ω_2 and ω_1 cross sections will not have uniform noise levels due to the inhomogeneous distribution pattern of the noise along the ω_3 axis. As a result, the spectral quality varies, depending on the type of cross section that is used. This can best be compared with the analysis of a 2D spectrum by means of 1D plots. The 2D frequency space can be visualized by slices perpendicular to the two frequency axes ω_1 and ω_2. In an ω_2 slice (a subspectrum in the ω_1 dimension) noise and resolution obscure the identification of cross peaks, whose intensities are only marginally higher than the noise level. On the other hand, cross peaks that can be identified are very reliable. To identify the marginal cross peaks, the ω_2 slice has to be compared with the ω_1 slice. In a similar fashion, we use all the different types of cross sections in the case of 3D NMR spectra.

As was noted before, the 3D NOE–HOHAHA experiment in principle contains the same information as the 3D HOHAHA–NOE experiment. However, due to the inhomogenous distribution of the noise in 3D spectra, there will be a difference between the two experiments. $C_{N\alpha N}$ connectivities are best identified in the ω_3 NH cross sections of the 3D NOE–HOHAHA experiments. As can be seen in Figure 7a, eight connectivities originate in the ω_1 NH cross section. This cross section will have a varying noise level in the 3D NOE–HOHAHA experiment, but in the 3D HOHAHA–NOE experiment the same information can be found in a "clean" ω_3 NH cross section.

3D cross peaks exhibit a certain line width in each dimension. This may lead to so-called "cross-talk", by which we mean that a cross peak may give rise to a residual peak in a cross section directly above or underneath it, or even in both cross sections. This slightly complicates the analysis of the data. However, checks can be made by comparing the cross sections with adjacent ones.

Results and Discussion

Spin System Analysis: Val 106. Four panels are shown in Figure 9 which illustrate the characterization of a valine spin system from a 3D NOE–HOHAHA spectrum of pike III parvalbumin in H_2O. Both the NH and the $C_\beta H$ resonance

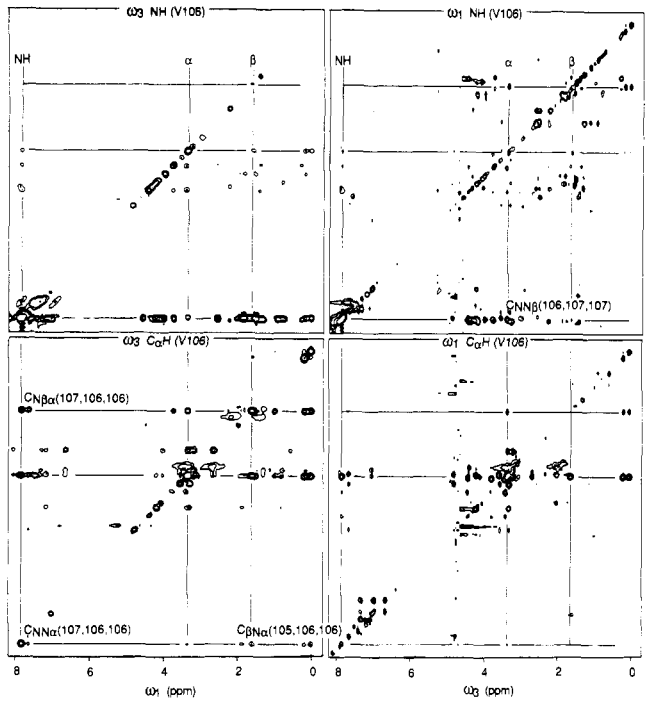

FIGURE 9: Cross sections perpendicular to the ω_1 and ω_3 axes of the 3D NOE–HOHAHA spectrum of pike III parvalbumin in H_2O. The two panels on the left display ω_3 cross sections at the NH and $C_\alpha H$ resonance frequencies of Val 106 from top to bottom, respectively, whereas the panels on the right display ω_1 cross sections at these frequencies. NH, $C_\alpha H$, and $C_\beta H$ resonance frequencies are indicated by solid lines. The C's of the sequential connectivity labels have been positioned in such a manner that each of them refers to the cross peak that lies above or under it.

fall in crowded regions of the spectrum. Thus, in the NH cross sections shown, cross peaks belonging to the amides of several residues will be present, in addition to cross-talk cross peaks. Also, the $C_\alpha H$ of Val 106 is known to have a chemical shift almost identical with that of the $C_\beta H$ of the neighboring His 107 (Padilla et al., 1988).

The ω_3 cross section at the NH frequency (uppermost left panel of Figure 9) serves as the starting point for the analysis of the spin system. The number of cross peaks in the $C_\alpha H$ region present on the HOHAHA line suggests that the amide proton overlaps with three to five amides of other residues. Assume, for instance, that one wishes to explore the spin system of the $C_\alpha H$ at 3.3 ppm, through which a horizontal α^{NOE} line has been drawn in the ω_3 NH cross section of Figure 9. The most likely candidates for the strong $C_{q\alpha N}(j,i,i)$ (q represents any other spin) connectivities in the aliphatic region of the α^{NOE} line are due to the intraresidue NOEs to the $C_\beta H$ or other aliphatic resonances. However, since these cross peaks result from NOE-transferred magnetization, they cannot be unambiguously assigned. The ω_1 NH cross section will then provide further information. The cross peaks on the horizontal α^J line at the $C_\alpha{}^H$ resonance frequency directly establish a connection $C_\alpha H$, $C_\beta H$, and further aliphatic protons (two small cross peaks). The presence of the back-transfer peak $C_{N\alpha N}$-(i,i,i) confirms the fact that this $C_\alpha H$ belongs to some NH with the resonance frequency of the cross section.

At a horizontal line at the presumed $C_\beta H$ frequency (the β^J line of the ω_1 NH cross section), the correlation between $C_\alpha H$, $C_\beta H$, and aliphatic protons is again established, but because of the absence of a back-transfer peak on this line, it could also be due to any NH aliphatic NOE.

Clearly, so far the NH, $C_\alpha H$, and $C_\beta H$ correlation, with further extension to two resonances in the methyl group region

(at 0.2 ppm), is already a strong indication for a valine spin system. At this stage, further checks to confirm this assignment can be made in the $C_\alpha H$ and $C_\beta H$ cross sections. The ω_3 and ω_1 cross sections at the $C_\alpha H$ frequency (left and right panels at the bottom of Figure 9, respectively) again establish at the horizontal β^{NOE} and β^J lines the correlation between the NH, $C_\alpha H$, $C_\beta H$, and aliphatic protons. Additionally, on the α^{NOE} and α^J lines in the ω_3 and ω_1 cross section at the $C_\beta H$ frequency (not shown), correlation between the NH, $C_\alpha H$, $C_\beta H$, and aliphatic protons was found. No new resonances were found. The sequence-specific assignment of these resonances to Val 106 follows in a later stage from the sequential analysis.

Identification of Sequential Connectivities of Val 106 to His 107 and Leu 105. Since the interresidue cross peaks in the NH region of the α^{NOE} line or β^{NOE} line in the ω_3 NH cross section are absent, other pathways indicated in Figures 5–7 need to be considered. The ω_1 plane at this frequency cannot be used since the four to six coinciding NH resonances prohibit a unique identification of the sequential steps. However, the ω_3 cross section at the $C_\alpha H$ frequency provides a solution (see bottom left panel to Figure 9). On the β^{NOE} line an extra cross peak in the NH region is found. A small cross peak with identical chemical shift (7.6 ppm) is also found on the NH^{NOE} line of the valine residue. These cross peaks correspond to the $C_{N\beta\alpha}(107,106,106)$ and $C_{NN\alpha}(107,106,106)$ connectivities, respectively. The $C_{N\beta\alpha}(107,106,106)$ connectivity is of particular importance since it is directional (Figure 5b), connecting Val 106 with its C-terminal neighbor, His 107. In addition, on the NH^{NOE} line in the $C_\alpha H$ cross section an NOE to a $C_\beta H$ is observed. The $C_{\beta N\alpha}(105,106,106)$ is expected in this region and must connect Val 106 with the preceding Leu 105. Both $C_{NN\alpha}(107,106,106)$ and $C_{\beta N\alpha}(105,106,106)$ can also be identified in an ω_2 cross section at the NH frequency of Val 106 (not shown). A confirmative cross peak $C_{NN\beta}(106,107,107)$ can be identified in the ω_1 cross section at the NH frequency of Val 106 (upper right panel of Figure 9). In spite of the severe overlap in the NH region of Val 106, these cross peaks establish the sequential connectivities with Leu 105 and His 107.

Sequential Assignment of Residues 54–63 of Parvalbumin. We shall now describe the sequential assignment of the peptide segment 54–63 of parvalbumin. This stretch contains a turn region (54–56) and regions of extended (57–59) and α-helical (60–63) conformation. The sequential assignment for these regions is illustrated in Figures 10–12, which also serve to show how the ω_1, ω_2, and ω_3 cross sections are used. Each panel of Figures 10–12 displays a ω_3, ω_1, or ω_2 NH cross section of the residue under consideration. Solid lines are used to illustrate correlation within one spin system, whereas broken lines are used to indicate sequential connectivities and hence connect different panels with each other.

Figure 10 shows the ω_3 NH cross sections of Ala 54–Ser 55–Gly 56 in the Ca-binding loop of parvalbumin. The $C_\alpha H$ and $C_\beta H_3$ of Ala 54 are easily identified. Simple spin systems such as alanines or glycines often serve as a starting point for the sequential assignment. The sequential connectivity $C_{N\alpha N}(55,54,54)$ is marked and allows a step to the ω_3 cross section of Ser 55 as is indicated by the broken line connecting this panel with the ω_3 NH(S55) panel.

In the first panel of Figure 10 one also observes an $i,i+2$ contact $C_{N\alpha N}(56,54,54)$ on the α^{NOE} line. As can be expected from the medium-range $d_{\alpha N}(i,i+2)$ NOE in turns, the 3D cross peak identifying this connectivity displays a weak intensity. This connectivity has also previously been characterized in 2D NMR studies (Padilla et al., 1988).

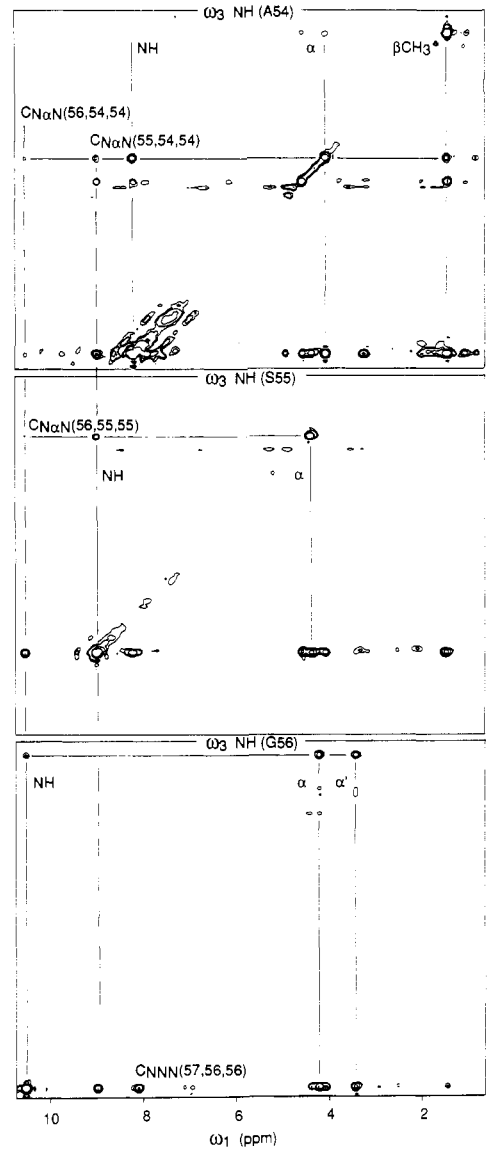

FIGURE 10: ω_3 NH cross sections of Ala 54–Ser 55–Gly 56 of the 3D NOE–HOHAHA spectrum of pike III parvalbumin in H_2O. The following convention is used for all panels: the ω_3 cross sections have a vertical ω_2 axis and a horizontal ω_1 axis. Solid lines are used to illustrate correlations within one spin system, whereas broken lines are used to indicate sequential connectivities and, hence, connect different panels. The C's of the connectivity labels have been positioned in such a manner that each of them refers to the cross peak that lies closest to it.

In the second panel of Figure 10 the ω_3 NH cross section of Ser 55 is depicted. Clearly, on the basis of this cross section alone no identification of the spin system can be made. However, the sequential steps $C_{N\alpha N}(56,55,55)$ and $C_{NNN}(56,55,55)$ are present, and they allow the step to the third panel of Figure 10. In effect, using such information corresponds to applying the main chain directed assignment strategy (Englander & Wand, 1987), which emphasizes the identification of NH, $C_\alpha H$, and $C_\beta H$ subspin systems and the establishment of their mutual connections on the basis of patterns expected for the various types of secondary structure elements.

The third panel of Figure 10 depicts the ω_3 cross section at the NH frequency of Gly 56. Both its C_α protons are readily identified, but no sequential 3D cross peaks could be found in this cross section. However, the $C_{NNN}(55,56,56)$ and $C_{NNN}(57,56,56)$ connectivities could be identified on the NOE line.

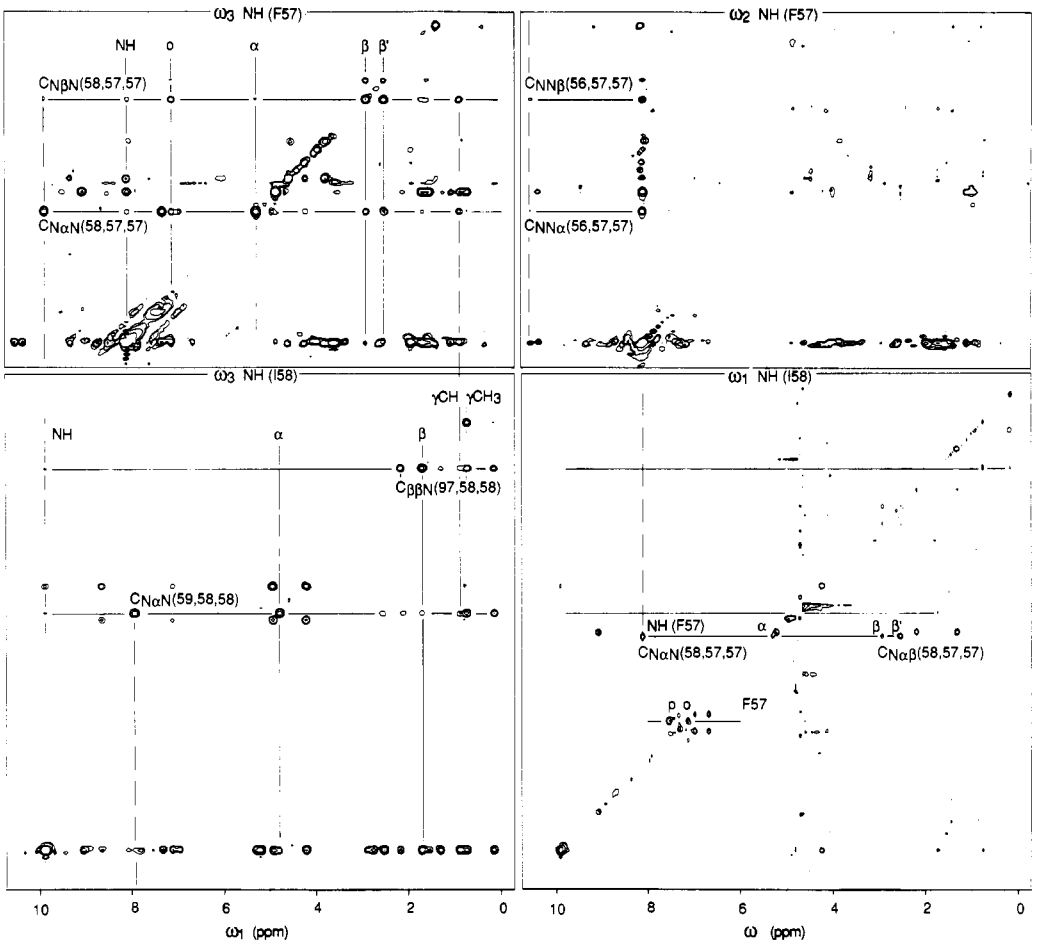

FIGURE 11: ω_3 and ω_1 or ω_2 NH cross sections of Phe 57 and Ile 58 of the 3D NOE–HOHAHA spectrum of pike III parvalbumin in H_2O. The orientation of the panels is such that in the ω_1 cross section the ω_2 axis is vertical and the ω_3 axis is horizontal, whereas in the ω_2 cross sections the ω_1 axis is vertical and the ω_3 axis horizontal. See caption of Figure 10 for the definition of the ω_3 cross sections. The C's of the connectivity labels have been positioned in such a manner that each of them refers to the cross peak that lies closest above or under it.

Figure 11 shows NH cross sections of Phe 57 and Ile 58. These residues have an extended backbone conformation, connecting the turn with the α-helical domain. The ω_3 cross section of Phe 57 is displayed in the top left-hand corner. The horizontal α^{NOE} line in the upper left panel of Figure 11 shows NOEs to the amide, ortho, $C_{\beta 1}$, and $C_{\beta 2}$ resonances of the Phe 57 spin system, and the sequential $C_{N\alpha N}(58,57,57)$ connectivity. On the β^{NOE} line, NOEs to the amide, ortho, C_α, and C_β protons are also seen together with the sequential $C_{N\beta N}$-(58,57,57) connectivity. On both lines connectivities to a $C_\gamma H$ of Ile 58 can be found, as is indicated by the broken line connecting the upper with the lower panel. The corresponding NOE $C_{\gamma\alpha}(58,57)$ of the connectivity $C_{\gamma\alpha N}(58,57,57)$ can be seen in the 2D NOE spectrum (Padilla et al., 1988). The NOE $C_{\beta\gamma}(57,58)$ cannot be unambiguously assigned by 2D NMR methods due to overlap, but the $C_{\gamma\beta N}(58,57,57)$ connectivity in the 3D spectrum firmly establishes its presence. The ω_2 panel at the NH resonance frequency of Phe 57 (upper right panel of Figure 11) is used to verify the sequential step Gly 56–Phe 57 through the connectivities $C_{NN\beta}(56,57,57)$ and $C_{NN\alpha}(56,57,57)$.

The sequential steps of the ω_3 cross section of Phe 57 connect this to the ω_3 cross section of Ile 58 (lower left panel of Figure 11). In this panel NOEs on the α^{NOE} and β^{NOE} lines show connectivities to the $C_\gamma H$, $C_\gamma H_3$, and $C_\delta H_3$ resonances of the spin system. The back-transfer peaks $C_{N\alpha N}(58,58,58)$ and $C_{N\beta N}(58,58,58)$ are also visible. The Ile 58 spin system can be traced via the $C_\delta H_3$, $C_\gamma H_3$, $C_\beta H$, and $C_\alpha H$ to NH. The remaining $C_\gamma H$ group is only connected by NOE to the $C_\beta H$. A strong sequential 3D cross peak $C_{N\alpha N}(59,58,58)$ is also found, which enables the sequential step to the NH cross section of Glu 59 to be made. An additional $\beta\beta$ cross peak on the β^{NOE} line of Ile 58, which was not previously identified in 2D NMR spectra due to overlap, is assigned as $C_{\beta\beta N}$-(97,58,58). In the ω_3 NH cross section of Ile 97 (not shown) the related $C_{\beta\beta N}(58,97,97)$ cross peak is also found. The ω_1 cross section of Ile 58 (lower right panel of Figure 11) gives the identification of the Phe 57 spin system in the ω_1 NH cross section of Ile 58. Indicated are the $C_{N\alpha N}(58,57,57)$ and $C_{N\alpha\beta}(58,57,57)$ connectivities. In addition, the ortho and para resonances of Phe 57 can be identified.

The Glue 59 ω_3 NH cross section also shows a strong $C_{N\alpha N}(60,59,59)$ connectivity (not shown). These strong $C_{N\alpha N}(i+1,i,i)$ and $C_{N\beta N}(i+1,i,i)$ connectivities in the stretch Phe 57–Glu 59 are indicative of an extended conformation of the molecule in this region (cf. Table I).

The sequential assignment of 54–58 of Figures 10 and 11 could be extended through the $C_{N\alpha N}(60,59,59)$ and C_{NNN}-(61,60,60) connectivities to Glu 61 (not shown). Figure 12 shows the NH cross sections of Glu 61–Lys 63 in helix D of parvalbumin. The ω_3 NH cross section (upper left panel of Figure 12) shows the back-transfer $C_{N\alpha N}(61,61,61)$ and the $C_{\gamma\alpha N}(61,61,61)$ and $C_{\beta\alpha N}(61,61,61)$ connectivities of the Glu 61 spin system. In the ω_1 NH cross section of Glu 61 (upper right panel of Figure 12) both the Glu 61 and the Glu 60 spin systems can be identified, the latter through the sequential $C_{N\alpha\beta}(61,60,60)$, $C_{N\alpha\gamma}(61,60,60)$, and $C_{N\beta\alpha}(61,60,60)$ connectivities. Moreover, the connection with the spin system of

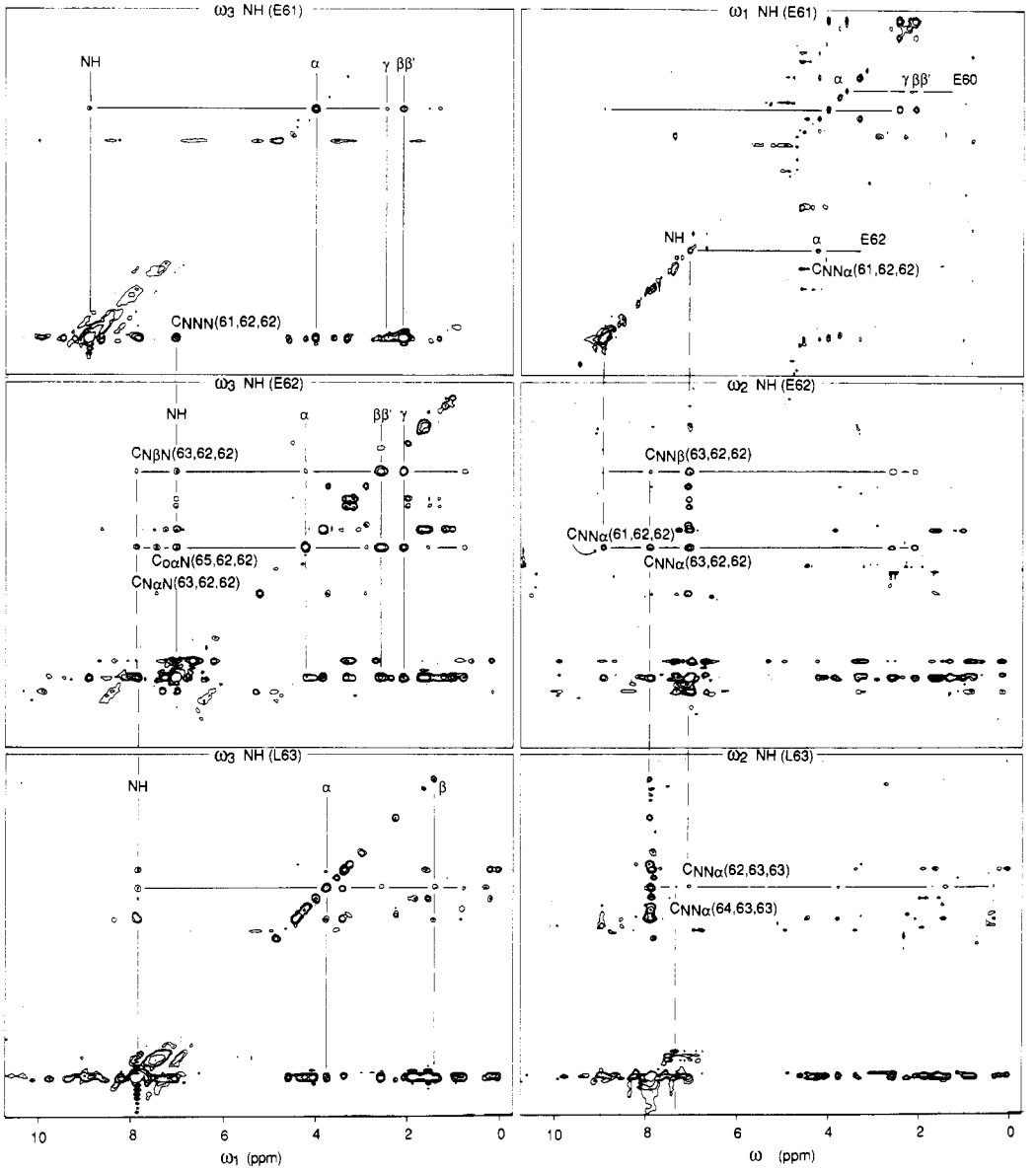

FIGURE 12: ω_3 and ω_1 or ω_2 NH cross sections of Glu 61, Glu 62, and Leu 63 of the 3D NOE–HOHAHA spectrum of pike III parvalbumin in H_2O. See captions of Figures 10 and 11 for definitions of the axes in the different cross sections. The C's of the connectivity labels have been positioned in such a manner that each of them refers to the cross peak that lies closest above or under it, unless indicated otherwise.

Glu 62 is made through the $C_{NN\alpha}(61,62,62)$ connectivity.

From the ω_3 cross section of Glu 61 the step to Glu 62 can also be made through a $C_{NNN}(61,62,62)$ contact. Both on the α^{NOE} line and on the β^{NOE} line in the ω_3 NH cross section of Glu 62 (middle left panel of Figure 12) intraresidue NOEs to all other resonances in the spin system can be seen. The sequential steps to Leu 63 are manifest as $C_{N\alpha N}(63,62,62)$ and $C_{N\beta N}(63,62,62)$ connectivities. Also an $i,i+3$ connectivity $C_{ortho,\alpha N}(65,62,62)$ to the ortho protons of Phe 65 can be identified. In the ω_2 NH cross section of Glu 62 (middle right panel of Figure 12) $C_{NN\alpha}(61,62,62)$ and $C_{NN\alpha}(63,62,62)$ sequential connectivities as well as the weaker $C_{NN\beta}(63,62,62)$ cross peak are visible.

The ω_3 NH cross section of Leu 63 is shown in the bottom left panel of Figure 12. Indicated are the amide, C_α, and C_β proton positions. The sequential connectivities $C_{NN\alpha}(62,63,63)$ and $C_{NN\alpha}(64,63,63)$ are found in the ω_2 cross section of Leu 63 (bottom right panel of Figure 12). Both the $i,i+3$ connectivity of Glu 62 and the presence of d_{NN}-based connectivities of Glu 61–Lys 63 are consistent with the α-helical conformation of this domain of the molecule (Padilla et al., 1988).

The relative 3D cross-peak intensities in secondary structure elements were given in Table I. From the analyzed data we can conclude that the cross peaks of the sequential connectivities generally have the predicted intensity.

Conclusions

The C notation for connectivities allows a convenient identification of cross peaks in the 3D frequency space. It represents a one-to-one mapping onto the observable coherence-transfer pathways of the molecules. This notation can easily be adapted to other types of 3D experiments and other (bio)molecules.

The analysis of the cross peaks in the 3D frequency space is most conveniently carried out in the ω_1, ω_2, and ω_3 cross sections perpendicular to the three frequency axes ω_1, ω_2, and ω_3. This was illustrated for the identification of a valine spin system from the 3D NOE–HOHAHA spectrum of pike III parvalbumin. Despite the fact that in both the NH and $C_\beta H$ regions considerable overlap was present, the combined use of the information of the ω_1 and ω_3 cross sections allowed the identification of all the spins in this valine residue.

On the basis of known short- and medium-range distances

in proteins for α-helices and β-sheets and long-range distances for β-sheet regions, we identified connectivities in proteins for the amide, C_α, and C_β protons. The intensities of the 3D cross peaks that correspond to these connectivities are strongly dependent on the secondary structure of the protein. We estimated the relative 3D cross-peak intensities for α-helical and β-sheet conformations. Strong 3D cross peaks are expected for $C_{\alpha N\alpha}$ and $C_{N\alpha N}$ connectivities in β-sheet domains, due to the favorable short proton–proton distance $d_{\alpha N}$ and the large $^3J_{\alpha N}$ coupling constant. In a stretch of extended backbone conformation of parvalbumin (residues 57–59), strong 3D cross peaks corresponding to these connectivities were indeed observed (Figure 11).

α-Helical domains are mainly characterized by $C_{NN\alpha}$ connectivities. Here the 3D cross-peak intensities are generally weaker. For the resdiues 60–63 in helix D of parvalbumin we observed 3D cross peaks corresponding to these connectivities (Figure 12).

In the nonselective 3D NOE–HOHAHA experiment or the related nonselective 3D HOHAHA–NOE, information about J-coupled protons and distance information for the sequential assignment are obtained from one dataset. For this reason, the complete assignment of a protein from one or two of these spectra should be possible. Such a procedure should preferably be implemented in automatic assignment algorithms. Automation of the assignment will be invaluable since the large number of cross peaks (10 000 or more) and the difficulties associated with displaying 3D datasets make a manual assignment of all cross peaks very tedious.

The increase in resolution can extend the range of biomolecules amenable to NMR studies beyond its current limit of about 15 000. This increase in resolution is illustrated by the identification of the novel NOEs $C_{\beta\beta N}$(97,58,58) and $C_{\gamma\beta N}$-(58,57,57), which are not observed in 2D NOE spectra due to overlap.

Some disadvantages of 3D NMR should also be mentioned. The experimental time needed for recording a spectrum is long, although some improvement can be made by omitting the dummy scans and reducing experimental time spent on I/O operations. The resulting large datasets require a substantial computing effort for processing. Finally, it should be realized that the experiment is dependent on the coherence transfer during the HOHAHA mixing period. The efficiency of this transfer is reduced with increasing size of the molecule, due to the increase in line width of the resonances. This imposes an inherent upper limit on the range of the technique. However, in the case of very large molecules, the 3D NOE–NOE experiment (Boelens et al., 1989) may become useful, since the efficiency of NOE transfer increases with increasing size of the molecules under study.

ACKNOWLEDGMENTS

We thank T. Schreurs for writing the interface software for transfer of the NMR data to the PS300 picture system.

REFERENCES

Bax, A., & Davis, D. G. (1985) *J. Magn. Reson. 65*, 355.
Boelens, R., Scheek, R. M., Dijkstra, K., & Kaptein, R. (1985) *J. Magn. Reson. 62*, 378.
Boelens, R., Vuister, G. W., Koning, T. M. G., & Kaptein, R. (1989) *J. Am. Chem. Soc. 111*, 8525.
Braunschweiler, L., & Ernst, R. R. (1983) *J. Magn. Reson. 53*, 521.
Davis, D. G., & Bax, A. (1985) *J. Am. Chem. Soc. 107*, 2850.
Englander, S. W., & Wand, A. J. (1987) *Biochemistry 26*, 5953.
Fesik, S. W., & Zuiderweg, E. R. P. (1988) *J. Magn. Reson. 78*, 588.
Griesinger, C., Sørensen, O. W., & Ernst, R. R. (1987a) *J. Magn. Reson. 73*, 574.
Griesinger, C., Sørensen, O. W., & Ernst, R. R. (1987b) *J. Am. Chem. Soc. 109*, 7227.
Hoffman, R. E., & Davies, D. B. (1988) *J. Magn. Reson. 80*, 337.
Kaptein, R., Boelens, R., Scheek, R. M., & van Gunsteren, W. F. (1988) *Biochemistry 27*, 5389.
Kessler, H., Gemmecker, G., & Steurnagel, S. (1988a) *Angew. Chem. 100*, 600.
Kessler, H., Gemmecker, G., Haase, B., & Steurnagel, S. (1988b) *Magn. Reson. Chem. 26*, 919.
Klevitt, R. E. (1985) *J. Magn. Reson. 68*, 551.
Marion, D., & Wüthrich, K. (1983) *Biochem. Biophys. Res. Commun. 113*, 967.
Marion, D., Kay, L. E., Sparks, S. W., Torchia, D. A., & Bax, A. (1989) *J. Am. Chem. Soc. 111*, 1515.
Noggle, J. H., & Schirmer, R. E. (1971) *The Nuclear Overhauser Effect, Chemical Applications*, Academic Press, New York.
Oschkinat, H., Griesinger, C., Kraulis, P. J., Sørensen, O. W., Ernst, R. R., Gronenborn, A. M., & Clore, G. M. (1988) *Nature 332*, 374.
Oschkinat, H., Cieslar, C., Gronenborn, A. M., & Clore, G. M. (1989) *J. Magn. Reson. 81*, 212.
Padilla, A., Cavé, A., & Parello, J. (1988) *J. Mol. Biol. 204*, 995.
Roberts, G. C. K., & Jardetzky, O. (1970) *Adv. Protein Chem. 24*, 447.
Vliegenthart, J. F. G., Dorland, L., & van Halbeek, H. (1983) *Adv. Carbohydr. Chem. Biochem. 41*, 209.
Vuister, G. W., & Boelens, R. (1987) *J. Magn. Reson. 73*, 328.
Vuister, G. W., Boelens, R., & Kaptein, R. (1988) *J. Magn. Reson. 80*, 176.
Vuister, G. W., de Waard, P., Boelens, R., Vliegenthart, J. F. G., & Kaptein, R. (1989) *J. Am. Chem. Soc. 111*, 772.
Wüthrich, K. (1986) *NMR of Proteins and Nucleic Acids*, Wiley, New York.
Wüthrich, K., Billeter, M., & Braun, W. (1984) *J. Mol. Biol. 180*, 715.
Zolnai, Z., Macura, S., & Markley, J. L. (1986) *Comput. Enhanced Spectrosc. 3*, 141.
Zuiderweg, E. R. P., & Fesik, S. W. (1989) *Biochemistry 28*, 2387.